JACS
JOURNAL OF THE AMERICAN CHEMICAL SOCIETY

Article

pubs.acs.org/JACS

Enantioselection on Heterogeneous Noble Metal Catalyst: Proline-Induced Asymmetry in the Hydrogenation of Isophorone on Pd Catalyst

Laura Rodríguez-García, Konrad Hungerbühler, Alfons Baiker, and Fabian Meemken*

Institute for Chemical and Bioengineering, Department of Chemistry and Applied Biosciences, ETH Zürich, Hönggerberg, HCI, CH-8093 Zürich, Switzerland

Supporting Information

ABSTRACT: In the (*S*)-proline-mediated asymmetric hydrogenation of isophorone (IP) on supported Pd catalyst, excellent enantioselectivity is achieved, with an enantiomeric excess of up to 99%. The role of the heterogeneous catalyst has been the subject of a controversial debate, and the current mechanistic understanding cannot explain the observed enantioselectivity of this catalytic system. The lack of *in situ* information about the role of the heterogeneous catalyst has prompted us to investigate the surface processes occurring at the methanol–Pd catalyst interface using attenuated total reflection infrared spectroscopy. Time-resolved monitoring of the homogeneous solution and of the catalytic solid–liquid interface coupled with catalytic data provides crucial information on the catalytically relevant enantiodifferentiating processes. While the condensation of IP and the corresponding chiral product 3,3,5-trimethylcyclohexanone with the chiral amine is connected to the enantiodifferentiation, it was found that the crucial enantioselectivity-controlling steps take place on the metal surface, and the reaction has to be classified as heterogeneous asymmetric hydrogenation. The presented spectroscopic and catalytic results provide strong evidence for the existence of two competing enantioselective processes leading to opposing enantioselection. Depending on surface coverage of the Pd catalyst, the reaction is controlled either by kinetic resolution ((*S*)-pathway) or by chiral catalysis ((*R*)-pathway). Steering the hydrogenation on the (*R*)-reaction pathway requires sufficient concentration of IP-(*S*)-proline condensate, as this chiral reactive intermediate becomes the most abundant surface species, inhibiting the competing kinetic resolution. The unraveled (*R*)-reaction pathway emphasizes an intriguing strategy for inducing chirality in heterogeneous asymmetric catalysis.

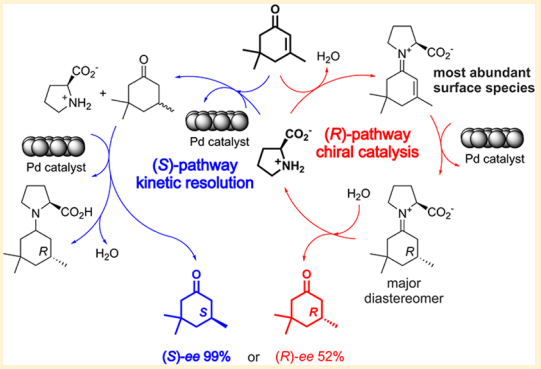

1. INTRODUCTION

Catalytic asymmetric hydrogenation is a key reaction in the production of optically active intermediates and products, which find important application as pharmaceuticals, agrochemicals, fragrances, and flavors.[1] While mostly homogeneous catalysts are employed for asymmetric hydrogenation, the application of heterogeneous catalysts could be beneficial due to their inherent practical advantages concerning catalyst stability, separation, and reuse. Furthermore, heterogeneous catalytic reactions are generally more amenable for continuous process operation. Prerequisite for the rational design of solid catalysts is a proper understanding of the structure of the active sites as well as of the mechanism of the chemical transformations occurring on the catalytic surface. Steering catalysis toward a desired pathway requires sophisticated strategies for controlling the environment at the catalytically active sites. Crucial for heterogeneous asymmetric catalysis is a chiral reaction environment, which directs the stereochemical orientation of the prochiral reactant on the active solid catalyst surface. This chiral reaction environment can be created by applying various strategies, including grafting, tethering, or encapsulation of active metal complexes with chiral ligands[2,3] or the strong adsorption of suitable chiral organic compounds.[4−6] While all these methods have been successfully applied, bestowing chirality to the surface by strongly adsorbing chiral compounds has proven to be most practical.

Simple addition of a small amount of a chiral compound, the so-called chiral modifier, to the liquid reaction solution is sufficient to induce strong stereochemical control in heterogeneous hydrogenations, exemplified by efficient asymmetric hydrogenations of α-activated ketones on cinchona-modified Pt and of α-functionalized olefins on cinchona-modified Pd.[4−6] For cinchona-modified Pt, the mechanistically best understood chirally modified metal, the established mechanistic models consider the active chiral modifier species to be strongly anchored to the Pt surface.[4−9] At such a chirally modified hydrogenation site, enantiodiscrimination originates from attractive interactions involving hydrogen bonding between the prochiral substrate and the tertiary amine moiety of the

Received: July 28, 2015
Published: September 2, 2015

DOI: 10.1021/jacs.5b07904
J. Am. Chem. Soc. 2015, 137, 12121−12130

adsorbed modifier,[10−12] leading to an enantiomeric excess (ee) of up to 98%.[13] The crucial role of hydrogen bonding between the prochiral reactant and the chiral modifier for enantiodifferentiation has recently been substantiated by attenuated total reflection infrared (ATR-IR) spectroscopic detection during the asymmetric hydrogenation.[12]

In the hydrogenation of the prochiral C=C bond in isophorone (IP) on supported Pd catalyst, addition of the chiral amino acid (*S*)-proline ((*S*)-Pr) to the liquid reaction solution also induces remarkable enantiodiscrimination, and an ee of up to 99% of the corresponding (*S*)-trimethylcyclohexanone (TMCH) has been reported (Scheme 1).[14] However, the

Scheme 1. Asymmetric Hydrogenation of Isophorone in the Presence of (*S*)-Pr on Pd Catalyst

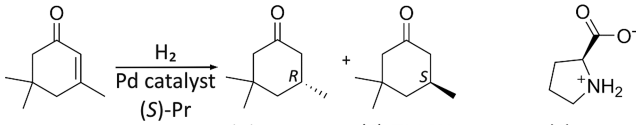

observed behavior of this catalytic system cannot be rationalized with the existing mechanisms proposed for chirally modified metals. The major difference is the large amount of chiral proline required to achieve high ee. According to catalytic data reported in the literature, enantioselectivity is also highly sensitive to other reaction parameters, e.g., the properties of the metal catalyst,[15] the catalyst support,[14,16] the solvent,[14] and even the preparation of the reaction solution.[17] The lack of *in situ* information about the surface processes occurring at the catalytic solid−liquid interface and contradictory experimental observations have led to a controversial debate on the origin of enantioselection in the hydrogenation of IP in the presence of (*S*)-Pr.[14,15,17−19] In 1989, Tungler et al. proposed enantioselectivity to result from stereoselective hydrogenation of an IP-(*S*)-Pr condensation product leading to the preferential formation of the (*S*)-enantiomer.[20,21] More recently, Lambert's group discovered preferential condensation of the cyclohexanone product (*R*)-TMCH with (*S*)-Pr in homogeneous solution and proposed kinetic resolution to be the sole origin of enantioselectivity. They also investigated the competitive adsorption of (*S*)-Pr and IP in an electrochemical study, and found the cyclohexenone to adsorb 10^5 times faster on a Pt electrode.[22] The authors extrapolated these findings, attempting to explain the surface processes occurring at the methanol−Pd catalyst interface, claiming that (*S*)-Pr is not able to translate chiral information to the surface reaction due to its very weak adsorption. In agreement with significantly stronger adsorption of IP, (*S*)-Pr was proposed to be exclusively present in the homogeneous reaction solution. Subsequent to the heterogeneous hydrogenation of IP to racemic TMCH, the chiral amino acid would then act as chiral resolving agent by forming preferentially (*R*)-TMCH-(*S*)-Pr condensate in the liquid phase. As the ee observed in the absence of Pd reaches only 8% (*S*)-TMCH, the role of the heterogeneous catalyst was further assigned to the reduction of TMCH-(*S*)-Pr condensate, thereby shifting the equilibrium to yield the unconsumed (*S*)-enantiomer in high excess.[17] If this is the underlying reaction mechanism, then the (*S*)-Pr-mediated asymmetric hydrogenation of IP on Pd catalyst cannot be classified as a *heterogeneous enantioselective* hydrogenation.

Addressing these claims, the groups of Török and Tungler published catalytic data which emphasized the strong effect of different Pd catalysts on the ee.[14,23] While they agreed on the importance of the kinetic resolution occurring in the liquid phase, their published results highlight the peculiar behavior of enantioselection during the course of the hydrogenation, which cannot be rationalized without the existence of an additional enantioselective pathway involving the Pd catalyst.

In addition to the debate on the underlying reaction mechanism, the synthetic aspect of the (*S*)-Pr-mediated enantioselective hydrogenation of IP has also been addressed. With the goal of achieving chiral modification of the heterogeneous catalyst, thiol derivatives of proline were anchored to the surface, but only very low ee (14%) was achieved.[24] Other approaches focused more on the role of the heterogeneous catalyst. Recently, catalytic systems using strongly basic support materials were proposed to promote (*S*)-Pr adsorption by ionic interactions between the chiral auxiliary and the catalyst support.[14] Particularly, carbonate-supported catalysts were claimed to promote high (*S*)-Pr coverage at the metal−support interface, which would inhibit racemic IP hydrogenation.[14] Furthermore, the effect of Pd particle size on various supports was investigated by Shen and co-workers, and a pronounced effect on the obtained enantioselectivity was found.[9] In another comprehensive study on the effect of Pd particle size of Pd/MgO catalysts, inversion of enantioselectivity with increasing Pd particle size was found.[15]

However, the current mechanistic understanding of the (*S*)-Pr-mediated hydrogenation of IP on Pd catalyst fails to explain these catalytic results. Particularly, the controversy over the role of the heterogeneous hydrogenation catalyst has hindered concerted research effort aiming at optimization and application of this system. For a more rational development of this complex but very intriguing enantioselective catalytic system, a better understanding of the origin of enantioselection is indispensable. The lack of *in situ* information on the role of the heterogeneous catalyst has prompted us to investigate the surface processes occurring at the catalytic solid−liquid interface using ATR-IR spectroscopy. Time-resolved monitoring of the homogeneous solution and of the methanol−Pd catalyst interface coupled with catalytic data provides crucial information on the catalytically relevant enantiodifferentiating processes. While the condensation of the cyclohexanone IP and the corresponding cyclohexanone TMCH with the chiral amine is connected to the enantiodifferentiation, it will be shown that, in fact, the surface coverage of the Pd catalyst controls the outcome of the asymmetric hydrogenation, and the crucial enantioselectivity-controlling steps take place on the metal surface. Based on our catalytic and spectroscopic results, we derived a new reaction pathway and completed the early proposed reaction scheme, which now can explain the existing published results. The unraveled reaction pathway emphasizes an intriguing strategy for inducing chirality in heterogeneous asymmetric catalysis.

2. EXPERIMENTAL SECTION

2.1. Materials. 3,5,5-Trimethyl-2-cyclohexene-1-one (Isophorone) (Aldrich, 97%), 3,5,5-trimethylcyclohexanone (Aldrich, 98%), (*S*)-Pr (Sigma-Aldrich, ≥99%), *N*-methyl-(*S*)-proline (Sigma-Aldrich), methanol (Sigma-Aldrich, 99.9%), 1-butanol (Merck, ≥99.5%), and propan-2-ol (Fisher, 99.95%) were used as received. Hydrogen (PanGas, Hydrogen 5.0, 99.999%) was used as received. Pure IP-(*S*)-Pr condensate (≥97% as determined by gas chromatography (GC))

DOI: 10.1021/jacs.5b07904
J. Am. Chem. Soc. 2015, 137, 12121−12130

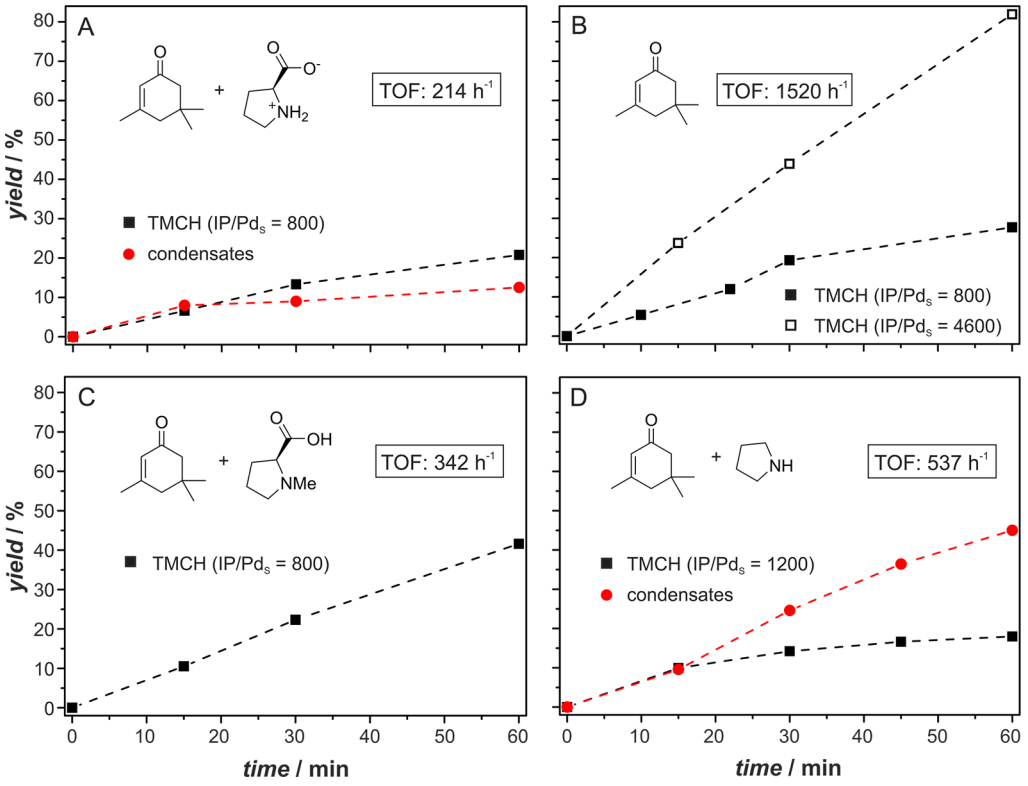

Figure 1. Yield of TMCH in the hydrogenation of IP on Pd/C catalyst in the presence of a stoichiometric amount of (*S*)-Pr (A), in the absence of (*S*)-Pr (B), and in the presence of stoichiometric amounts of (*S*)-NMePr (C) and pyrrolidine (D). The formation of condensation products is indicated in red.

was obtained by separation of an equilibrated IP-(*S*)-Pr solution (≥60% IP conversion) using column chromatography.

The commercial 5 wt% Pd/C (5000 Engelhard, Pd dispersion: 0.53) and 5 wt% Pd/Al_2O_3 (76002 Fluka, Pd dispersion: 0.46) were used as received. Preparation of a 5 wt% Pd/TiO_2 catalyst (Pd dispersion: 0.27) has been described elsewhere,[25] and prior to use this catalyst was reduced in a fixed-bed tubular reactor under flowing hydrogen for 30 min at room temperature. Dispersion was determined by CO chemisorption.

2.2. Hydrogenations. Hydrogenations of IP were performed in a 50 mL three-necked glass reactor at 298 K (controlled by a Mettler Toledo Easy Max 102) and at atmospheric pressure under a constant flow of H_2 (semi-batch hydrogenation). The general reaction procedure was the following: The catalyst was transferred to the reactor and reduced *in situ* in 6 mL of solvent under constant H_2 flow for 1 h. The reaction was then initiated by addition of an IP, BuOH (internal standard), and (*S*)-Pr reaction mixture in 10 mL of solvent. The following reaction conditions were used for all hydrogenations unless stated otherwise: 8.0 ± 0.1 mg of 5 wt% Pd catalyst, 100 mM IP (1.6 mmol), 100 mM (*S*)-Pr (modifier: Pd_s, 850:1), 16 mL of solvent, 298 K, hydrogen flow, and mechanical stirring (500 rpm). Studies on the kinetic resolution of TMCH were conducted according to the same procedure except that TMCH was used instead of IP. Racemic hydrogenation of IP was performed with 5.0 ± 0.1 mg of 5 wt% Pd catalyst, 100 mM IP (8.0 mmol), 80 mL of solvent, room temperature, hydrogen flow, and mechanical stirring (900 rpm). The conversion and enantioselectivity were determined by GC using a flame ionization detector and a chiral capillary column (CP-Chirasil-Dex CB, 25 m length, 0.25 mm internal diameter, 0.25 μm film thickness). The conversion of IP was calculated using butanol as internal standard.

2.3. Preparation of Pd/C Thin Films for ATR-IR. A slurry was prepared with Pd/C catalyst (2 mg) and deionized water (2 mL), which was ultrasonicated for 15 min to obtain a well-mixed suspension. Subsequently, the entire amount of the slurry was placed on a ZnSe internal reflection element (IRE, bevel of 45°, 72 mm × 10 mm × 6 mm, Specac Ltd.), and water was evaporated at 353 K for 2 h. This procedure yielded a catalyst layer of 1.5 ± 0.1 mg. After the coated crystal was mounted in a flow-through cell, the catalyst layer was reduced by subjecting it to flowing solvent saturated with hydrogen at 298 K for 1 h prior to use. The as-prepared catalyst layer adhered to the IRE such that, after initial material loss of loosely adhered Pd/C particles, no further ablation of catalyst was observed over the course of several hours under flow-through conditions.

2.4. ATR-IR Spectroscopy. ATR-IR spectra were recorded on a Bruker 70v spectrometer equipped with a liquid nitrogen cooled MCT detector. A home-built stainless steel flow-through cell mounted on an ATR-IR attachment (OPTISPEC) was used for all measurements. Spectra were recorded at 4 cm^{-1} resolution. The measurement temperature (298 K) was regulated by a thermostat (Julabo, F25). The home-built flow-through cell and its implementation into a recycle reactor have been described in detail elsewhere.[26]

Modulation excitation spectroscopy (MES) experiments were carried out by changing between two different solutions every 3 min. The cycles were repeated several times to obtain stable responses of active species, and the last three cycles were integrated into one cycle to average the spectra and to enhance the signal-to-noise ratio.

3. RESULTS AND DISCUSSION

3.1. Hydrogenation Activity of IP in the Presence of (*S*)-Pr and (*S*)-Pr Derivatives. Kinetic resolution of racemic TMCH by enantioselective condensation of (*S*)-Pr and (*R*)-TMCH in the *homogeneous* phase is proposed to be responsible for the enantioselection in the hydrogenation of IP and is currently the accepted reaction mechanism in the literature.[17] According to this mechanism, IP has to be rapidly hydrogenated on Pd to racemic TMCH, and subsequently the (*R*)-enantiomer is enantioselectively consumed by condensation with (*S*)-Pr in the liquid phase. The condensation, however, is limited by competing hydrolysis, but a consecutive reduction

DOI: 10.1021/jacs.5b07904
J. Am. Chem. Soc. 2015, 137, 12121−12130

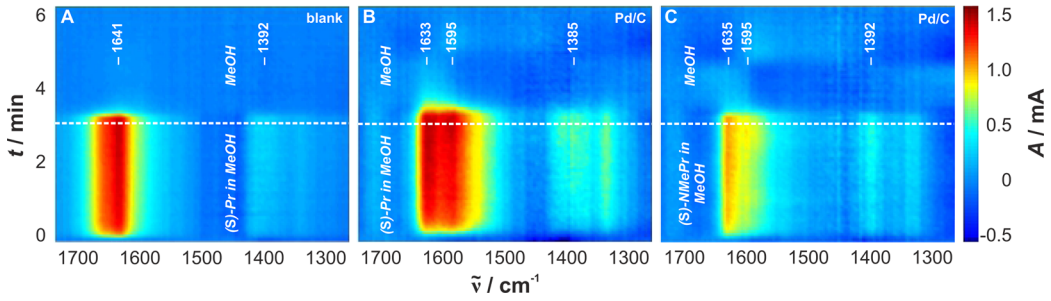

Figure 2. Time-resolved surface spectra during concentration modulation between 1 and 0 mM (*S*)-Pr in methanol on a blank internal reflection element (IRE) (A) and on a Pd/C-coated IRE (B), and between 1 and 0 mM (*S*)-NMePr solution on Pd/C-coated IRE (C) at 298 K. The modulation period was set to 3 min, and three modulation cycles were averaged.

on the Pd catalyst, yielding the fully saturated (*R*)-TMCH-(*S*)-Pr adduct, is proposed to complete the kinetic resolution *in the liquid phase* with a maximum yield of 50% (*S*)-TMCH.

In preliminary experiments using freshly prepared reaction solutions (within 1 min prior to initiation of hydrogenation), we also observed an ee of (*S*)-TMCH and obtained a turnover frequency (TOF) of 214 h^{-1}. Interestingly, in the absence of (*S*)-Pr, a significantly higher TOF of 1520 h^{-1} was obtained (Figure 1B). In contrast to the proposed displacement of (*S*)-Pr and strong abundance of the cyclohexenone on the catalytic surface,[22] such a pronounced drop in catalytic activity does indicate strong interference of the chiral amino acid with the fast hydrogenation of IP. Note that our Pd/C catalyst displays superior performance compared to the values reported in the literature,[9,27] but a similar effect on the catalytic activity was also observed with less active catalysts.

To better understand the molecular interaction(s) of (*S*)-Pr with the reactant and with the Pd catalyst, and to identify the decisive factors leading to the deterioration of the hydrogenation activity, we carried out IP hydrogenations in the presence of proline derivatives. The effect of competitive liquid-phase condensation on the TOF was investigated using the tertiary amine *N*-methyl-(*S*)-proline ((*S*)-NMePr), which cannot form condensation products. Adding a stoichiometric amount of (*S*)-NMePr to the hydrogenation of IP also led to a significant drop in TOF (Figure 1C). Nevertheless, the tertiary amine did not induce any enantioselection, indicating the crucial role of the secondary amine for the enantioselection. For the hydrogenation in the presence of pyrrolidine (Py), a TOF of 537 h^{-1} was achieved. However, TMCH formation significantly decreased after 30 min, while the condensation of IP and Py led to ongoing consumption of IP (Figure 1D).

From the catalytic activities presented in Figure 1, we infer that (*S*)-Pr does interfere with the hydrogenation of IP due to competitive interaction in the liquid phase and on the catalytic surface, which involves the adsorption of (*S*)-Pr and condensation products. While no condensates were formed in the presence of (*S*)-NMePr, the nearly 5 times reduced hydrogenation rate indicates that the acid can competitively adsorb on the Pd catalyst. In a reflection absorption infrared spectroscopic study under ultra-high-vacuum conditions, Raval et al. have found strong adsorption of (*S*)-Pr on Cu(110) via the carboxylate moiety and the nitrogen of the amino group.[28] Considering the observed effect of (*S*)-NMePr on catalytic activity, sufficiently strong interaction via the carboxylate with the Pd catalyst appears to also occur under hydrogenation conditions in the presence of methanol. Another crucial observation concerns the influence of IP-Py condensate formation and its effect on the catalytic reaction (Figure 1D). From the ceasing TMCH formation rate, we infer that such condensate products are prone to accumulate on the catalytic surface, which then leads to blocking of active IP hydrogenation sites.

3.2. Adsorption of IP and (*S*)-Pr on Pd Catalyst in the Presence of Methanol. For a more comprehensive understanding on the role of (*S*)-Pr in the hydrogenation of IP on Pd catalyst in methanolic solution, we attempted to monitor the catalytic solid–liquid interface under reaction conditions by means of *in situ* ATR-IR spectroscopy. However, alumina-supported catalysts, normally preferred for such studies due to the strong adherence of alumina on the IRE, proved to be unsuitable for studying this catalytic system. First of all, among the tested catalysts, the alumina-supported catalysts performed poorly, independent of the catalyst pretreatment. Furthermore, in ATR-IR adsorption experiments using Pd/Al_2O_3 catalyst layer, no adsorption from IP-containing methanol solution was discernible. In contrast, strong adsorption of (*S*)-Pr on this catalyst was detected, but the control experiment with an Al_2O_3 layer confirmed accumulation of the amino acid on the support material. To obtain spectroscopic data relevant to the processes occurring at the methanol–Pd interface, we developed a layer deposition technique suitable for making a sufficiently stable Pd/C catalyst layer (see Experimental Section). Not only does the Pd/C catalyst provide by far the best catalytic performance, but also the investigated adsorbates do not dynamically adsorb and desorb on carbon within the time constant of the experiments, which significantly facilitates spectral analysis of the surface processes occurring on Pd.

In Figure 2, time-resolved surface plots display the vibrational changes monitored on a blank (panel A) and on a Pd/C-coated (panels B,C) internal reflection element (IRE) during switching from H_2-saturated methanol solution to H_2-saturated methanol solution containing either (*S*)-Pr (panels A,B) or (*S*)-NMePr (panel C). For all experiments, continuous switching between the two solutions in 3 min intervals revealed that the detected species were captured in quasi-steady state; that is, appearance and disappearance of absorption signals modulated between maximum and minimum intensities within this time scale. To improve the signal-to-noise ratio of the low-intensity absorption bands, the quasi-steady-state data were averaged over several runs, which in the literature is referred to as concentration modulation excitation spectroscopy (MES).[29,30]

On blank IRE, the liquid-phase absorption of 1 mM (*S*)-Pr in methanol was detected. The broad and intense $\nu_{as}(OCO^-)$ of zwitterionic (*S*)-Pr peaked at 1641 cm^{-1}. A second broad absorption band peaking at around 1392 cm^{-1} was discernible,

DOI: 10.1021/jacs.5b07904
J. Am. Chem. Soc. 2015, 137, 12121–12130

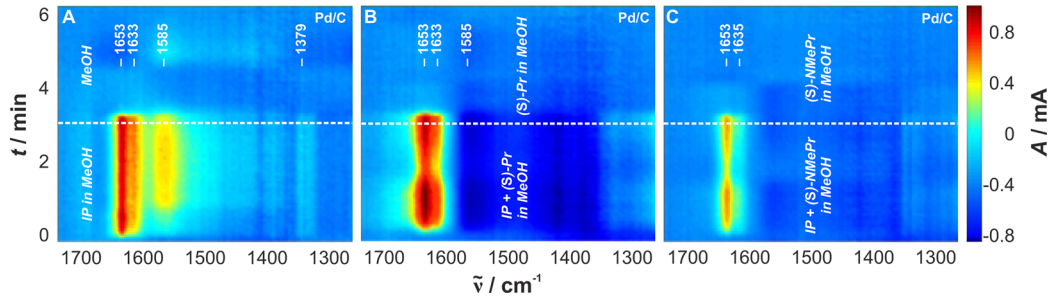

Figure 3. Time-resolved surface spectra during concentration modulation between 1 and 0 mM IP in methanol (A), 1 and 0 mM IP in a 1 mM (*S*)-Pr methanolic solution (B), and 1 and 0 mM IP in a 1 mM (*S*)-NMePr methanolic solution (C) on Pd/C-coated IRE at 298 K. The modulation period was set to 3 min, and three modulation cycles were averaged.

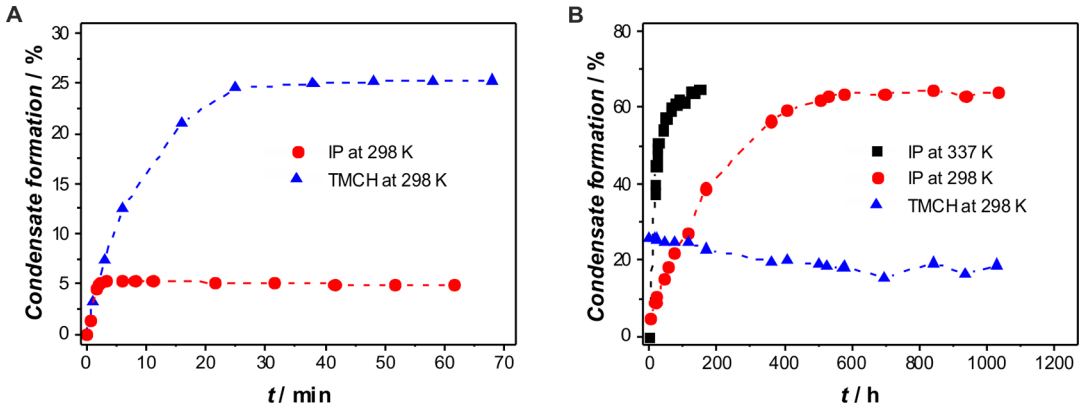

Figure 4. Formation of condensates in methanolic stoichiometric mixtures of IP and (*S*)-Pr as well as racemic TMCH and (*S*)-Pr (160 mM), followed within 60 min using *in situ* ATR-IR spectroscopy (A) and followed until complete equilibration using GC (B).

which corresponds to a combination of $\nu_s(OCO^-)$ and $\delta(C-H)$.[31] On Pd/C-coated IRE (Figure 2B), the center of the $\nu_{as}(OCO^-)$ was red-shifted to 1633 cm^{-1}, and the $\nu_s(OCO^-)$ was blue-shifted to 1385 cm^{-1}. Another spectral feature on Pd/C-coated IRE was detected at 1595 cm^{-1}, which we assign to the carbonyl bond of adsorbed formyl species originating from partially dehydrogenated methanol. The additional MES experiment using He- and H_2-saturated methanol solutions corroborated this assignment as the signal grew in the absence of H_2 (compare Figure S1 in Supporting Information). Detection of formyl species upon admission of amino acid as well as tailing of the $\nu_{as}(OCO^-)$ band upon switching back to pure methanol revealed that (*S*)-Pr interacts with Pd under reaction conditions. Furthermore, shifting of the carboxylate absorption bands indicates interaction of the amino acid with the Pd catalyst via the carboxylate moiety. Comparing the surface spectra of the secondary and tertiary amines in Figure 2, panels B and C, respectively, weaker adsorption of (*S*)-NMePr on Pd was found. While the $\nu_{as}(OCO^-)$ was also shifted upon interaction with the Pd catalyst, weaker band intensities and slower formation of formyl species suggest weaker interaction of the tertiary amine.

In the concentration MES experiment shown in Figure 3A, adsorption of IP on Pd/C in the absence of (*S*)-Pr is depicted. Upon interaction of IP with the Pd catalyst, the ratio of C═O (1653 cm^{-1}) to C═C (1633 cm^{-1}) stretch absorption was attenuated compared to the absorption of dissolved IP (compare Figure S2 in Supporting Information), suggesting a rather parallel orientation of the ketone bond with respect to the metal surface (Greenler's surface selection rule[32]). However, the observed adsorption strength of IP was similar to that in the case of (*S*)-Pr concentration MES, both accumulating only rather weakly at the methanol–Pd interface.

Their competitive adsorption is emphasized in the surface spectra in Figure 3B, which displays the spectral changes induced by switching the feed from H_2-saturated methanol solution containing 1 mM (*S*)-Pr to H_2-saturated methanol solution containing 1 mM (*S*)-Pr and 1 mM IP. Compared to the surface spectra involving only IP (Figure 3A), the co-adsorption of (*S*)-Pr led to significant broadening and stronger absorption in the C═O stretch region, which might originate from intermolecular interactions as well as dynamic re-orientation of the reactants with respect to the catalytic Pd surface. As no significant attenuation of the $\nu_{as}(OCO^-)$ mode of (*S*)-Pr was discernible, detection at the methanol–Pd interface reveals a cooperative rather than a competitive interaction between the prochiral cyclohexenone and the amino acid. Instead of displacement of (*S*)-Pr, co-adsorption of IP seems to be at the expense of adsorbed formyl species, followed by the compensated absorption at 1585 cm^{-1}. Stronger adsorption of the chiral amino acid involving only its carboxylate moiety is further supported by the surface spectra, emphasizing the co-adsorption of IP and (*S*)-NMePr. Upon addition of IP, no negative signals assignable to the tertiary amine are detected, while the signal intensity of the ketone carbonyl is less pronounced (compare Figure 3, panels A and C).

In agreement with the catalytic results obtained with (*S*)-Pr and its derivatives, the spectroscopic data provide evidence that (*S*)-Pr is able to interfere on the catalytic Pd surface with the hydrogenation of IP in methanolic solution.

DOI: 10.1021/jacs.5b07904
J. Am. Chem. Soc. 2015, 137, 12121–12130

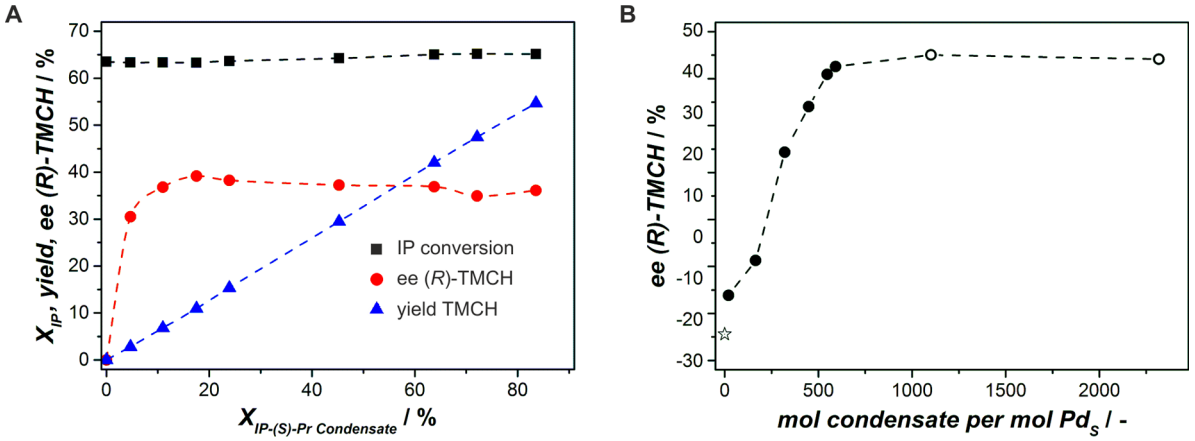

Figure 5. (A) Conversion of IP, yield of TMCH, and ee as a function of consumed IP-(*S*)-Pr condensate using equilibrated IP-(*S*)-Pr solution and 8.0 mg of Pd/C catalyst. (B) Influence of the molar ratio of IP-(*S*)-Pr condensate to Pd_S on ee (determined after 60 min hydrogenation) using pre-equilibrating reaction solutions. Solid circles denote the standard procedure described in the Experimental Section, while the experiments corresponding to the two open circles were performed with 4 and 2.2 mg of catalyst, respectively. The star indicates kinetic resolution starting with racemic TMCH.

3.3. Homogeneous Condensation Reactions. As condensation in the liquid phase is proposed to play a crucial role for enantiodifferentiation, we studied methanolic reaction solutions in the absence of Pd catalyst using ATR-IR spectroscopy and chiral GC analysis. Upon mixing of IP and (*S*)-Pr (both 160 mM) in the reaction vessel, a rapid decrease of the IP carbonyl stretch at 1651 cm^{-1} was observed, indicating the formation of condensate (Figure 4A). The carbonyl signal decreased by 5% within less than 10 min and remained constant thereafter. A sample was drawn after 30 min, and 5% conversion of the cyclohexenone, corresponding to the formation of 8 mM IP-(*S*)-Pr condensate, was confirmed by GC analysis. For a stoichiometric mixture of racemic TMCH and (*S*)-Pr, the carbonyl band of the cyclohexanone at 1705 cm^{-1} decreased by 25% within 30 min, indicating the formation of 40 mM TMCH-(*S*)-Pr condensate. Thereafter, the consumption of TMCH ceased and did not change substantially during the following 60 min. Again, GC analysis confirmed TMCH consumption of 25%. However, the GC analysis also showed that 14.5% of (*R*)-TMCH and 10.0% of (*S*)-TMCH were consumed, revealing the poor enantioselection (6% ee (*S*)-TMCH) of the liquid-phase condensation in its thermodynamic equilibrium. Considering the time constants of the catalytic experiment (ca. 18 h) and of the rather rapid equilibration (ca. 30 min), kinetically controlled kinetic resolution in the liquid phase can also be ruled out as the origin of the very high enantioselectivity. Instead, enantioselection must be governed by a different mechanism.

As the preparation of the liquid reaction solution has been reported to strongly influence the outcome of the catalytic reaction, we investigated the equilibrating liquid phase of stoichiometric methanolic mixtures containing 160 mM ketone and (*S*)-Pr stored under air at room temperature over several days (Figure 4B). Samples were drawn in regular intervals, and the extent of condensation was measured by GC using butanol as internal standard. Continuous consumption of cyclohexenone was observed, reaching the thermodynamic equilibrium at 67% conversion. At 337 K, the thermodynamic equilibrium was reached significantly faster. It will be shown below that the IP-(*S*)-Pr condensate formed is the chiral reactive intermediate leading to chiral catalysis in the asymmetric hydrogenation of IP. As also shown in Figure 4B, the kinetics of cyclohexanone condensation is very different, as the thermodynamic equilibrium is reached within the initial 30 min. The TMCH-(*S*)-Pr condensate even slowly hydrolyzed during the course of a month, which is very likely caused by air moisture entering through the pierced GC vial, but the ee remained constant at 6 ± 1%.

3.4. Heterogeneous Hydrogenation of IP-(*S*)-Pr Condensate. In order to grasp the importance of the IP-(*S*)-Pr condensate for the reaction mechanism, we performed hydrogenations with pre-equilibrated reaction mixtures on Pd/C. Strikingly, inversion of enantioselectivity was observed; that is, an ee of around 40% (*R*)-TMCH was obtained. As shown in Figure 5A, the ee remained almost constant for 5 h. Notice that the initial IP conversion − obtained through homogeneous condensation − remained constant throughout the hydrogenation. Only after a reaction time of 24 h was additional minor conversion (2%) of IP observed. Therefore, we propose that IP-(*S*)-Pr condensate strongly accumulates on the Pd surface, blocking IP from accessing free hydrogenation sites. In addition, the absence of fully saturated TMCH-(*S*)-Pr adducts in the reaction mixture sampled during the experiment suggests that both (*R*)- and (*S*)-TMCH-(*S*)-Pr condensates are rapidly replaced from the catalytic surface by more strongly adsorbing IP-(*S*)-Pr condensate. On the basis of the results presented in Figure 5, we conclude that the IP-(*S*)-Pr intermediate has to be the most abundant surface species, adsorbing significantly more strongly on the Pd surface than its hydrogenation products and the reactant IP.

Moreover, hydrogenations with increased content of IP-(*S*)-Pr condensate (standard reaction solution with prolonged premixing time) showed an excellent correlation between obtained ee of (*R*)-TMCH and the used molar ratio of IP-(*S*)-Pr condensate to Pd surface (Pd_S) (Figure 5B). Therefore, we propose that the crucial enantioselectivity-controlling steps do take place on the catalytic surface, and chiral IP-(*S*)-Pr intermediate is able to dictate the outcome of the catalytic reaction by inhibiting hydrogenation of TMCH-(*S*)-Pr condensates. The significant contribution of the formation of IP-(*S*)-Pr condensate and the competitive formation of (*R*)-TMCH, even in the hydrogenation using fresh IP-(*S*)-Pr-reaction solution, are also highlighted in Figure 5B by the enantioselectivity obtained in the reaction of racemic TMCH

DOI: 10.1021/jacs.5b07904
J. Am. Chem. Soc. 2015, 137, 12121−12130

and (*S*)-Pr. In the absence of IP, 10% higher (*S*)-excess is observed after 60 min, showing that initially fast formation of cyclohexene condensate (compare section 3.3) is able to compete with the mechanism leading to the preferential formation of (*S*)-TMCH. When the surface is fully saturated with IP-(*S*)-Pr condensate, the best enantioselectivity to (*R*)-TMCH is achieved. Using 2.2 mg instead of 8 mg of catalyst, we obtained the best ee of 52% (*R*)-TMCH after 240 min, corroborating the strong influence of high IP-(*S*)-Pr condensate surface coverage.

To investigate the structure sensitivity of the Pd catalyst and the influence of the support material, hydrogenations of equilibrated IP-(*S*)-Pr solutions were also performed on Pd/Al_2O_3, Pd/TiO_2 and pre-reduced Pd/C catalysts (Table 1).

Table 1. Catalytic Results Using Several Different Pd Catalysts for Fresh and Equilibrated Reaction Solutions[a]

		fresh solutions		equil. solutions	
catalyst	dispersion	TOF	(*S*)-ee	TOF	(*R*)-ee
Pd/C untreated	53%	214 h^{-1}	14%	102 h^{-1}	40%
Pd/C reduced	13%	347 h^{-1}	15%	252 h^{-1}	52%
Pd/Al_2O_3	46%	60 h^{-1}	9%	153 h^{-1}	39%
Pd/TiO_2	27%	321 h^{-1}	9%	1144 h^{-1}	33%[b]

[a]The TOF and ee were determined after 15 and 60 min, respectively. [b]The ee started declining after 15 min (ee 51%) due to high conversion of IP-(*S*)-Pr condensate.

Independent of the pre-treatment of the catalyst or the support material used, an ee of (*R*)-TMCH was always obtained with the equilibrated reaction solution, whereas hydrogenations using fresh reaction solution always gave the (*S*)-enantiomer in excess. Interestingly, under otherwise identical reaction conditions, increasing the Pd particle sizes of the Pd/C catalyst by reductive treatment at 400 °C for 1 h significantly enhanced the ee from 40 to 52% (*R*)-TMCH and doubled the TOF. Using a Pd/Al_2O_3 catalyst, the same ee as for non-pre-treated Pd/C but a higher activity were obtained. An exceptional activity for the IP-(*S*)-Pr condensate hydrogenation was experienced with our Pd/TiO_2 catalyst, yielding also an enantioselectivity of 51% ee. The influence of particle size on enantioselectivity and the very high TOF found for the titania-supported catalyst demonstrate the potential for optimizing the performance of this catalytic system.

3.5. Adsorption of Condensates on Pd/C. Finally, we investigated the adsorption of condensates at the methanol–Pd catalyst interface. Due to the dynamic nature of the condensation equilibria in liquid solution and competing hydrolysis of condensates (compare section 3.3), we decided to implement the ATR-IR flow-through cell into a recycle reactor setup (3 mL volume)[26] to follow adsorption at the solid–liquid interface from a liquid reaction solution in dynamic equilibrium. After reduction of the deposited Pd/C catalyst layer for 1 h using H_2-saturated methanol, a stable background was obtained, and condensate-containing solutions were fed to the recycle reactor.

For investigating the adsorption of IP-(*S*)-Pr condensate, purified inlet solution was prepared employing column chromatography. Within 27 s at a flow rate of 11 mL/min, the recycle reactor content was quickly exchanged with H_2-saturated methanol solution containing 3.7 mM IP-(*S*)-Pr condensate and approximately 0.4 mM IP as well as 0.4 mM (*S*)-Pr. As seen in the surface spectra presented in Figure 6A, broad absorption bands centered at 1366, 1549, and 1609 cm^{-1} grew continuously during recycling, which is highlighted for the latter absorption mode in the inset. After 33 min (red spectrum), accumulation on the catalyst had ceased, and flushing of the recycle reactor with H_2-saturated methanol revealed the detection of species strongly bound to Pd/C (blue spectrum). In comparison to the adsorption experiments using pure IP and (*S*)-Pr (compare section 3.2), these absorption bands were also significantly broadened and appeared at shifted positions, evidencing high surface coverage by another species, namely IP-(*S*)-Pr condensate adsorbed to Pd/C. However, among the different IP-(*S*)-Pr condensate species (imine, diene, ketone) proposed in the literature,[20,23] no unambiguous distinction was possible due to the broad nature of the absorption bands.

Nevertheless, to confirm stronger adsorption of IP-(*S*)-Pr condensate at the methanol–Pd interface, we also investigated the adsorption of TMCH-(*S*)-Pr condensate. The fast hydrolysis makes it very difficult to isolate this condensate in methanol. Therefore, an inlet solution containing 10 mM racemic TMCH and 10 mM (*S*)-Pr was equilibrated under H_2 atmosphere for 60 min, yielding 2.5 mM TMCH-(*S*)-Pr condensate. As seen in Figure 6B, quick exchange of the recycle reactor content induced increasing absorption at 1365, 1630, and 1705 cm^{-1}. The latter absorption mode is assignable to the

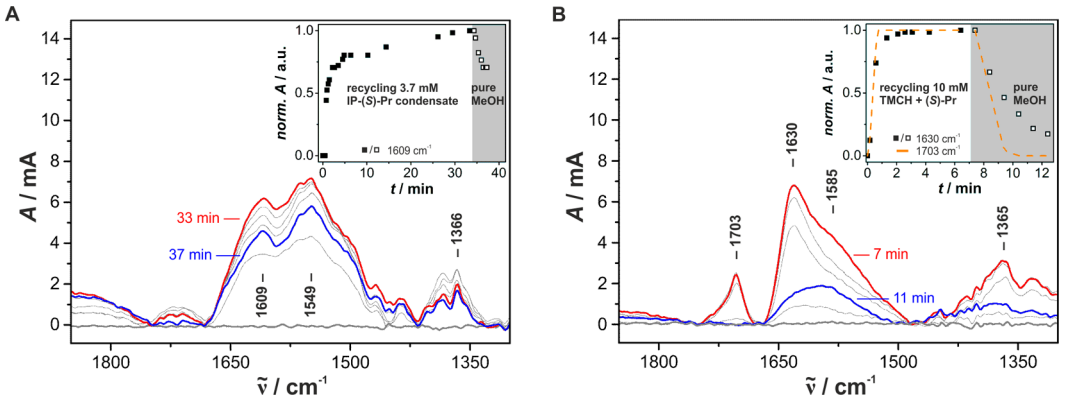

Figure 6. Adsorption on Pd/C from 3 mL of H_2-saturated methanol solution containing 3.7 mM IP-(*S*)-Pr condensate (A) and 2.5 mM TMCH-(*S*)-Pr condensate (B). Due to the competing hydrolysis in liquid phase, 0.4 mM IP and 0.4 mM (*S*)-Pr (A) as well as 7.5 mM TMCH and 7.5 mM (*S*)-Pr (B) were also present in the inlet solutions.

DOI: 10.1021/jacs.5b07904
J. Am. Chem. Soc. 2015, 137, 12121–12130

Scheme 2. Enantioselectively Competing Reaction Pathways Involving Kinetic Resolution ((*S*)-Pathway) and Chiral Catalysis ((*R*)-Pathway) for the (*S*)-Pr-Mediated Asymmetric Hydrogenation of IP on Supported Pd Catalyst

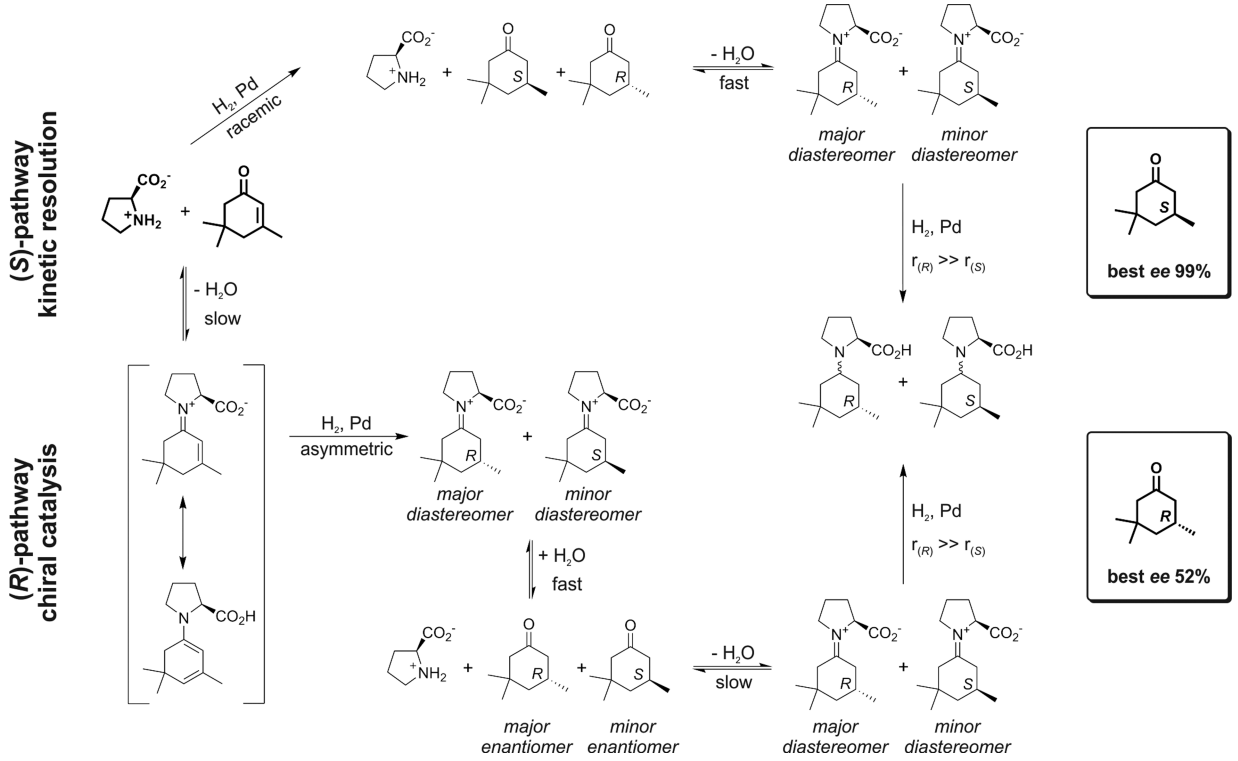

carbonyl band of TMCH, which did not change after 2 min. The other two absorption modes obeyed slightly slower kinetics, reaching saturation within 3 min. The broad absorption centered at 1630 cm^{-1} can originate from residual (*S*)-Pr and from TMCH-(*S*)-Pr condensate accumulating on Pd, but no isolated peak indicating only the adsorption of the latter was discernible. After saturation of the catalyst (red spectrum), the recycle reactor was again flushed with H_2-saturated methanol for 4 min (blue spectrum). Compared to the adsorption of IP-(*S*)-Pr condensate, the detected species were removed significantly faster, revealing their relatively weak adsorption. Note that also adsorbed formyl species have to contribute to the remaining absorption centered at 1585 cm^{-1}.

In agreement to the catalytic results presented in section 3.4, the surface spectra provide evidence for the strong accumulation of IP-(*S*)-Pr condensate on Pd. In contrast, IP, (*S*)-Pr, TMCH, and TMCH-(*S*)-Pr condensates seem to interact only weakly with the catalyst. While the active surface species leading to enantiodifferentiation toward the (*R*)-enantiomer could not be identified, the crucial role of IP-(*S*)-Pr condensate for controlling access to the heterogeneous catalyst was corroborated by the spectroscopic analysis.

3.6. Mechanistic Implications and Proposed Reaction Scheme. The presented catalytic and spectroscopic results provide strong evidence for the existence of two competing enantioselective processes leading to opposing enantioselection in the Pr-mediated asymmetric hydrogenation of IP on Pd-supported catalyst. Furthermore, we propose that the crucial enantioselectivity-controlling steps occur on the heterogeneous catalyst, and even the earlier discovered kinetic resolution is governed by a stereoselective hydrogenation on Pd. Depending on surface coverage of the Pd catalyst, enantioselection is controlled either by kinetic resolution ((*S*)-pathway) or by chiral catalysis ((*R*)-pathway). The two competing reaction pathways presented in Scheme 2 can explain the outcome of the catalytic hydrogenation, and the decisive reaction parameter determining the sense of enantioselection is the concentration of IP-(*S*)-Pr condensate formed in the first equilibrium involving IP and (*S*)-Pr.

Following the (*S*)-pathway in Scheme 2, hydrogenation of IP in the presence of (*S*)-Pr without pre-equilibration favors kinetic resolution, and the amino acid will mainly act as chiral resolving agent. While competitive adsorption of (*S*)-Pr and continuous IP-(*S*)-Pr condensate formation interfere with the efficient catalysis governed by this reaction pathway, the cyclohexenone IP is still hydrogenated on Pd to racemic TMCH. In the liquid phase, the condensation between (*S*)-Pr and both enantiomers of the cyclohexanone rapidly reaches equilibrium, consuming slightly more (*R*)-TMCH, leading to an enantiomeric ratio of 150:133 in favor of (*S*)-TMCH. However, the crucial enantiodifferentiating step in the kinetic resolution is the diastereoselective hydrogenation of the (*R*)-TMCH-(*S*)-Pr condensate on the Pd catalyst. Fast hydrogenation of the (*R*)-(*S*)-diastereomer on Pd catalyst drives the equilibrium toward full consumption of (*R*)-TMCH, and the significantly slower hydrogenation of the (*S*)-TMCH-(*S*)-Pr condensate ($r_{(R)} \gg r_{(S)}$ in Scheme 2) enables efficient kinetic resolution, leading to very high enantioselectivity of (*S*)-TMCH. The most efficient kinetic resolution would be achieved by addition of (*S*)-Pr after the fast racemic hydrogenation of IP. Deterioration of activity due to the competitive adsorption of the chiral resolving agent on active hydrogenation sites would be avoided, and lower yield due to the preferential formation of the other (*R*)-enantiomer would be prevented in the absence of any IP-(*S*)-Pr condensate. Nevertheless, undesired consumption of 50% of the prochiral

DOI: 10.1021/jacs.5b07904
J. Am. Chem. Soc. 2015, 137, 12121−12130

starting material IP as well as an equivalent molar amount of resolving agent (*S*)-Pr limits the maximum yield to 50% (*S*)-TMCH, which is the main drawback of this pathway.

From an economic and environmental point of view, chiral catalysis is a more elegant approach to produce only one enantiomer of a chiral compound, because a small amount of chiral catalyst is able to induce optical activity in a large amount of product and formation of the undesired enantiomer is avoided. Following the (*R*)-pathway in Scheme 2, true heterogeneous asymmetric catalysis is achieved in the hydrogenation of IP on supported Pd using (*S*)-Pr as chiral modifier. The crucial reaction parameter for steering the hydrogenation on this pathway is the concentration of the chiral reactive intermediate IP-(*S*)-Pr, which can control the availability of active hydrogenation sites. If the molar ratio of IP-(*S*)-Pr condensate to Pd_S is sufficiently high (IP-(*S*)-Pr condensate to Pd_S exceeding roughly 700 for Pd/C), the chiral reactive intermediate becomes the most abundant surface species, blocking surface access for any other species present in the liquid reaction solution. While it remains an open question whether the catalytically active IP-(*S*)-Pr condensate surface species is the imine or the diene species, its hydrogenation on Pd catalyst leads to the preferential formation of (*R*)-TMCH-(*S*)-Pr condensate. Following the stereoselective hydrogenation, both diastereomers, the major (*R*)- and the minor (*S*)-TMCH-(*S*)-Pr condensate, are quickly replaced by the more strongly adsorbing IP-(*S*)-Pr enantiomer, preventing the consecutive kinetic resolution. Fast hydrolysis of the cyclohexane condensates in liquid solution yields the ee of (*R*)-TMCH, and also the chiral modifier (*S*)-Pr is recovered. Steering the hydrogenation on the (*R*)-pathway, we obtained an ee of 52% (*R*)-TMCH. However, optimization with respect to the reaction conditions, the properties of the heterogeneous hydrogenation catalyst, the support material, and the molecular structure of the chiral modifier provide plenty of opportunities to maximize the enantioselection. In addition, sophisticated exploitation of both reaction pathways allows for combining the benefits of chiral catalysis and kinetic resolution. While chiral catalysis using (*S*)-Pr as chiral modifier produces an enantio-enriched reaction solution with higher efficiency, subsequent kinetic resolution employing (*R*)-Pr as resolving agent allows for obtaining (*R*)-TMCH with optical purity.

Furthermore, the discovered pathway for the (*S*)-Pr-mediated asymmetric hydrogenation of IP employing the amino acid as chiral modifier emphasizes an intriguing strategy for translating chiral information to an originally racemic heterogeneous hydrogenation of a prochiral substrate. The general strategy for imprinting a chiral selector onto the prochiral substrate to achieve heterogeneous asymmetric catalysis is summarized in Scheme 3: Initially, a chiral, amine-based modifier rapidly condensates with the prochiral α,β-unsaturated ketone to form a chiral reactive intermediate (step I). The obtained enantiomer preferentially adsorbs with one of its two enantiofaces on the Pd catalyst (step II), which represents the enantiodifferentiating step of the catalytic cycle. In step III, hydrogenation of the chiral alkene leads to the preferential formation of one of the two diastereomeric alkanes, which upon desorption (step IV) hydrolyze in the liquid phase to yield the chiral product alkane and to recover the chiral modifier for the next enantioselective catalytic cycle (step V). Tuning electronic and steric properties of the chiral modifier is one of the crucial parameters to allow for an efficient enantioselective catalytic turnover. However, the lack of

Scheme 3. Proposed Strategy for Translating Chiral Information to an Originally Racemic Heterogeneous Hydrogenation of a Prochiral Substrate

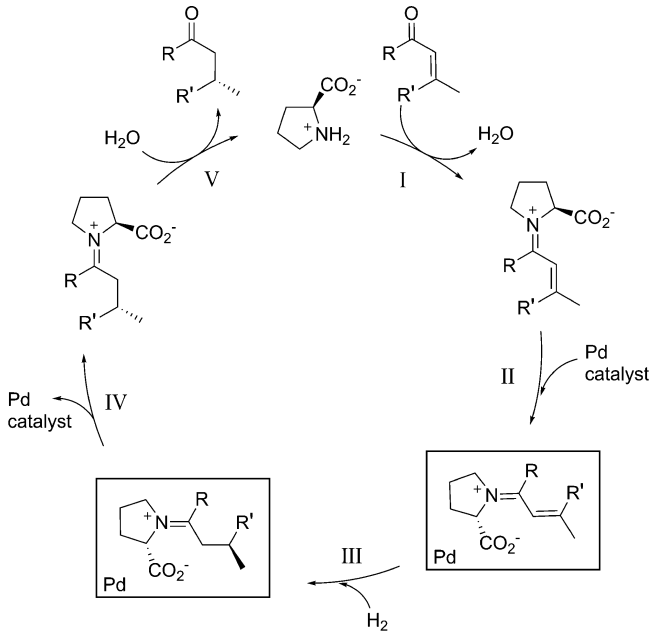

information about the exact molecular structure of the catalytically active IP-(*S*)-Pr condensate does not allow for distinguishing between electronic and steric effects responsible for controlling the enantiospecific adsorption of the condensate intermediate, and further mechanistic understanding is required to optimize such stereoselective hydrogenations in a more rational way.

4. CONCLUSIONS

We have investigated the reaction steps occurring in the bulk liquid phase and on the metal surface during the (*S*)-Pr-mediated hydrogenation of IP over supported Pd catalysts. The combined catalytic and spectroscopic studies revealed the existence of two competing reaction pathways: kinetic resolution resulting in the production of (*S*)-TMCH, and Pd-catalyzed stereoselective hydrogenation of IP-(*S*)-Pr condensate leading to (*R*)-TMCH. The revisited reaction mechanism not only explains the existing controversial interpretation of the origin of enantioselectivity, but also answers the long-standing debate about the role of the Pd catalyst for enantioselection. The slowly forming condensate between IP and (*S*)-Pr is a key reaction intermediate in the reaction scheme owing to its ability to block active hydrogenation sites. Furthermore, it is stereoselectively hydrogenated on Pd catalyst. The preferentially formed (*R*)-TMCH-(*S*)-Pr condensate hydrolyzes rapidly in the liquid phase with residual water and thus leads to the observed ee of (*R*)-TMCH.

An intriguing general strategy for translating chiral information to a heterogeneously catalyzed reaction can be drawn from the discovered reaction pathway. In contrast to chirally modified metal catalysts, chiral information is imprinted onto the substrate by simple condensation of an α,β-unsaturated carbonyl group and a secondary amine carrying the chiral information. The resulting unsaturated chiral condensate is prone to adsorb enantiospecifically on the heterogeneous catalyst and controls access to the catalytically active sites. After the asymmetric transformation of the chiral

DOI: 10.1021/jacs.5b07904
J. Am. Chem. Soc. 2015, 137, 12121−12130

reactive intermediate, scission of the chiral modifier by hydrolysis yields the chiral product.

■ ASSOCIATED CONTENT

Supporting Information

The Supporting Information is available free of charge on the ACS Publications website at DOI: 10.1021/jacs.5b07904.

Experimental details, time-resolved surface spectra during modulation between H_2- and He-saturated methanol, liquid-phase IR spectrum of a methanolic IP solution, CO chemisorption procedure, and TEM images of Pd/C and Pd/TiO_2 catalysts (PDF)

■ AUTHOR INFORMATION

Corresponding Author

*fabian.meemken@chem.ethz.ch

Notes

The authors declare no competing financial interest.

■ ACKNOWLEDGMENTS

We thank Dr. Robert Büchel for the CO chemisorption measurements and Dr. Frank Krumeich for the TEM measurements. Financial support by the Foundation Claude & Giuliana is kindly acknowledged.

■ REFERENCES

(1) Ager, D. J.; de Vries, A. H. M.; de Vries, J. G. *Chem. Soc. Rev.* **2012**, *41*, 3340.
(2) McMorn, P.; Hutchings, G. J. *Chem. Soc. Rev.* **2004**, *33*, 108.
(3) De Vos, D. E.; Vankelecom, I. F. J.; Jacobs, P. A. *Chiral catalyst immobilization and recycling*; Wiley-VCH: Weinheim, 2000.
(4) Mallat, T.; Orglmeister, E.; Baiker, A. *Chem. Rev.* **2007**, *107*, 4863.
(5) Studer, M.; Blaser, H. U.; Exner, C. *Adv. Synth. Catal.* **2003**, *345*, 45.
(6) Bartók, M. *Curr. Org. Chem.* **2006**, *10*, 1533.
(7) Lavoie, S.; Laliberte, M. A.; Temprano, I.; McBreen, P. H. *J. Am. Chem. Soc.* **2006**, *128*, 7588.
(8) Zaera, F. *J. Phys. Chem. C* **2008**, *112*, 16196.
(9) Zhan, E. S.; Li, S.; Xu, Y. D.; Shen, W. J. *Catal. Commun.* **2007**, *8*, 1239.
(10) Bonalumi, N.; Bürgi, T.; Baiker, A. *J. Am. Chem. Soc.* **2003**, *125*, 13342.
(11) Demers-Carpentier, V.; Goubert, G.; Masini, F.; Lafleur-Lambert, R.; Dong, Y.; Lavoie, S.; Mahieu, G.; Boukouvalas, J.; Gao, H.; Rasmussen, A. M. H.; Ferrighi, L.; Pan, Y.; Hammer, B.; McBreen, P. H. *Science* **2011**, *334*, 776.
(12) Meemken, F.; Hungerbühler, K.; Baiker, A. *Angew. Chem., Int. Ed.* **2014**, *53*, 8640.
(13) Sutyinszki, M.; Szöri, K.; Felföldi, K.; Bartók, M. *Catal. Commun.* **2002**, *3*, 125.
(14) Mhadgut, S. C.; Török, M.; Esquibel, J.; Török, B. *J. Catal.* **2006**, *238*, 441.
(15) Li, S.; Chen, C. H.; Zhan, E. S.; Liu, S. B.; Shen, W. J. *J. Mol. Catal. A: Chem.* **2009**, *304*, 88.
(16) Schäfer, C.; Mhadgut, S. C.; Kugyela, N.; Török, M.; Török, B. *Catal. Sci. Technol.* **2015**, *5*, 716.
(17) McIntosh, A. I.; Watson, D. J.; Burton, J. W.; Lambert, R. M. *J. Am. Chem. Soc.* **2006**, *128*, 7329.
(18) Kyriakou, G.; Beaumont, S. K.; Lambert, R. M. *Langmuir* **2011**, *27*, 9687.
(19) Szabados, E.; Györffy, N.; Tungler, A.; Balla, J.; Könczöl, L. *React. Kinet., Mech. Catal.* **2014**, *111*, 107.
(20) Tungler, A.; Kajtar, M.; Máthé, T.; Toth, G.; Fogassy, E.; Petró, J. *Catal. Today* **1989**, *5*, 159.
(21) Tungler, A.; Máthé, T.; Petró, J.; Tarnai, T. *J. Mol. Catal.* **1990**, *61*, 259.
(22) McIntosh, A. I.; Watson, D. J.; Lambert, R. M. *Langmuir* **2007**, *23*, 6113.
(23) Györffy, N.; Tungler, A.; Fodor, M. *J. Catal.* **2010**, *270*, 2.
(24) Watson, D. J.; Jesudason, R.; Beaumont, S. K.; Kyriakou, G.; Burton, J. W.; Lambert, R. M. *J. Am. Chem. Soc.* **2009**, *131*, 14584.
(25) Huck, W. R.; Bürgi, T.; Mallat, T.; Baiker, A. *J. Catal.* **2001**, *200*, 171.
(26) Meemken, F.; Müller, P.; Hungerbühler, K.; Baiker, A. *Rev. Sci. Instrum.* **2014**, *85*, 17.
(27) Mhadgut, S.; Török, M.; Dasgupta, S.; Török, B. *Catal. Lett.* **2008**, *123*, 156.
(28) Mateo Marti, E.; Barlow, S. M.; Haq, S.; Raval, R. *Surf. Sci.* **2002**, *501*, 191.
(29) Baurecht, D.; Fringeli, U. P. *Rev. Sci. Instrum.* **2001**, *72*, 3782.
(30) Urakawa, A.; Bürgi, T.; Baiker, A. *Chem. Eng. Sci.* **2008**, *63*, 4902.
(31) Bieri, M.; Bürgi, T. *ChemPhysChem* **2006**, *7*, 514.
(32) Greenler, R. G.; Snider, D. R.; Witt, D.; Sorbello, R. S. *Surf. Sci.* **1982**, *118*, 415.

DOI: 10.1021/jacs.5b07904
J. Am. Chem. Soc. 2015, 137, 12121−12130